Arabian Journal of Chemistry (2016) 9, 854–864

King Saud University

Arabian Journal of Chemistry

www.ksu.edu.sa
www.sciencedirect.com

ORIGINAL ARTICLE

"One-pot" synthesis of fluorescent Au@SiO_2 and SiO_2@Au nanoparticles

Nicoleta Liliana Olteanu [a,1], Cosmina Andreea Lazăr [a,1], Adina Roxana Petcu [a,1], Aurelia Meghea [a,1], Elena Adina Rogozea [a,*], Maria Mihaly [b,*]

[a] *University Politehnica of Bucharest, Research Centre for Environmental Protection and Eco-friendly Technologies, Polizu 1, RO-011061 Bucharest, Romania*
[b] *University Politehnica of Bucharest, Faculty of Applied Chemistry and Materials Science, Inorganic Chemistry, Physical Chemistry and Electrochemistry Department, Polizu 1, RO-011061 Bucharest, Romania*

Received 28 October 2015; accepted 19 December 2015
Available online 2 January 2016

KEYWORDS

Core–shell plasmonic nanostructure;
Microemulsion technique;
"One-pot" procedure;
Dye fluorescence enhancement

Abstract A class of fluorescent Au@SiO_2 and SiO_2@Au core–shell fluorescent nanoparticles has been synthesized using microemulsion assisted sol–gel method coupled with photoreduction reaction as an easy, rapid and versatile "one-pot" procedure. In the case of Au@SiO_2-RhB (gold nanoparticles core coated with silica-Rhodamine B shell) different silica shell sizes were obtained ranging from 3 to 116 nm, while for RhB-SiO_2@Au (Rhodamine B-silica core coated with gold nanoparticles shell) the size of gold shell falls within 3–38 nm interval. The synthesized core–shell nanoparticles have been characterized by a variety of techniques including Dynamic Light Scattering (DLS), High-Resolution Transmission Electron Microscopy (HR-TEM) coupled with Energy-Dispersive X-ray spectroscopy (EDX), Scanning Electron Microscopy (SEM), X-ray Diffractometry (XRD) and UV–VIS–NIR spectroscopy to confirm the size, shape, stability and topographic structure of the both core–shell nanostructures. The fluorescence enhancement of Rhodamine B (RhB) dye in the presence of gold nanoparticles (AuNPs) was demonstrated for the core–shell nanostructures synthesized in the present study, for different silica or gold shells. These interesting fluorescent core–shell nanoparticles provide ideal candidates for a variety of applications in materials science, biology, catalysis and optical fields.

* Corresponding authors. Tel./fax: +40 213154193.
E-mail addresses: adinarogozea@gmail.com (E.A. Rogozea), maria.mihaly@upb.ro (M. Mihaly).
[1] Tel./fax: +40 213154193
Peer review under responsibility of King Saud University.

ELSEVIER Production and hosting by Elsevier

1. Introduction

A promising and important approach in the development of fluorescent nanoparticles for technological and biomedical applications is represented by the metal-enhanced fluorescence (MEF) nanoparticles. The interaction between the excited-state of fluorophores and free electrons (surface plasmon electrons) in the metal nanoparticles can result in enhanced optical properties, such as: fluorescence enhancement, potentiated fluorophore photostability, increased quantum yield, and

http://dx.doi.org/10.1016/j.arabjc.2015.12.014
1878-5352

reduced lifetime of the fluorophores (Geddes and Lakowicz, 2002; Wang et al., 2011, 2008a,b). Fluorescent dye molecules in close proximity with metallic nanoparticles have shown modified optical properties which are found to be dependent on: (i) size, shape and capping layer of the metallic nanoparticles; (ii) the extent of spectral overlap of localized surface plasmon resonance (LSPR) band with the absorption and emission bands of the dye and (iii) their cationic or anionic nature (Amjadi and Farzampour, 2014; Narband et al., 2009; Sen and Patra, 2009, 2008). For example, gold nanoparticles (AuNP) and Rhodamine 6G (Rh 6G) dyes are metallic nanoparticle dye composite systems in which the LSPR band of Au nanoparticles (530 nm) significantly overlaps with absorption (550 nm) and emission (579 nm) bands of the dye. Such a synergistic combination is very useful for many applications like: surface enhanced Raman scattering (SERS) (Chen et al., 2007a; Rigo et al., 2011), photostability (Dong et al., 2011) and enhancement of fluorescent dye (Sathiyamoorthy et al., 2011), random lasing (Dong et al., 2012; Popov et al., 2006), photoinduced morphological changes (Chandrasekharan et al., 2000), resolution imaging (Larson et al., 2003), single molecule detection and biological labelling (Kinkhabwala et al., 2009).

Different concentrations of AuNPs lead to modified dye fluorescence intensity, excited state lifetime and Raman scattering of the dye molecules. The enhancement or quenching of the fluorescence dye depends on the distance between the metallic surface and the fluorescent molecules. Therefore, coating the metal nanoparticles with a suitable silica shell is a useful method to keep the fluorescent molecules at a certain distance from the metal. The silica shell surrounding the gold core has several important purposes: limits the effect of the outer environment (such as oxygen, certain solvents, and soluble species in buffer solutions) on the fluorescent dye contained in the nanoparticles, protects the metal core against corrosion when the particles are subjected to electrolyte solution, acts as an insulator to avoid charge recombination within the metal, gives a better thermal stability preventing the sintering of the gold cores and adjusts the plasmon dye separation distance to minimize quenching (Törngren et al., 2014). More importantly, the entrapment enhances the hydrophilicity, biocompatibility and stability of the metal nanoparticles and fluorescent dye under physiological conditions (Knopp et al., 2009; Rossi et al., 2005; Yan et al., 2007). The nanoparticles exhibit little or no cytotoxicity, which makes them promising for *in vivo* observation of cell trafficking and tumour targeting as well as for disease diagnosis and treatment (Luo et al., 2004; Zhu et al., 2004).

Fluorescent nanoparticles as metal-enhanced fluorescence can be synthesized by using different methods including sol–gel condensation (Popov et al., 2006), chemical deposition (Sen and Patra, 2009), layer-by-layer synthesis (Amjadi and Farzampour, 2014), seed induced deposition (Sen and Patra, 2008), sonochemical process (Dong et al., 2012), electroless plating (Chandrasekharan et al., 2000; Chen et al., 2007b) and reverse microemulsion method (Lu et al., 2013; Pak and Yoo, 2013; Ren et al., 2015), etc. In all these approaches the fabrication of nanoshells is often a multi-step, time consuming process which requires a strict control of each step in order to obtain structures with desired properties. Therefore, the monitoring of their thickness and homogeneity still remains a very difficult task. Herein is proposed an easy, rapid, "one-pot" method for the synthesis of $Au@SiO_2$ and $SiO_2@Au$ core–shell fluorescent nanoparticles with a homogeneous structure.

The present paper reports, for the first time, a convenient and versatile "one-pot" procedure by water-in-oil microemulsion assisted sol–gel method combined with photoreduction reaction which allows the obtaining of both $Au@SiO_2$-RhB (gold nanoparticles core coated with silica-Rhodamine B shell) and RhB-$SiO_2@Au$ (Rhodamine B-silica core coated with gold nanoparticles shell) core–shell fluorescent nanoparticles with a homogeneous structure. The thickness of the silica and gold shell can be controlled by changing the conditions of the synthesis process such as the volume of TEOS or the gold precursor. The Dynamic Light Scattering (DLS), Transmission Electron Microscopy (TEM), High-Resolution Transmission Electron Microscopy (HR-TEM), Selected Area Diffraction (SAED), Scanning Electron Microscopy (SEM), X-ray Diffraction (XRD) and Energy-Dispersive X-ray Spectroscopy (EDX) were used to confirm the size, shape, structure and stability of the both core–shell nanostructures. The effects of either silica or gold shell on the fluorescence of Rhodamine B dye were investigated. This study is important as fluorescent $Au@SiO_2$ nanoparticles are widely used in imaging and drug delivery (Hayashi et al., 2013), while fluorescent $SiO_2@Au$ nanoparticles found applications in fluorescence sensor as valuable tools in biochemistry and medicine, mainly because of its sensitivity and simplicity. In particular, the sensors based on fluorescence resonance energy transfer between donor and acceptor have been used to bioanalysis, such as micro RNA, protein and ion (Miao et al., 2016).

2. Materials and methods

2.1. Materials

Tetrachloroauric acid trihydrate ($HAuCl_4{\cdot}3H_2O$, 99.9%), polyoxyethylene-4-lauryl ether (Brij 30), sodium 3-sulfonate mercaptopropane (3-MS), tetraethoxysilane (TEOS), (3-aminopropyl) trimethoxysilane (APTMOS), 2,2,4-trimethypentan (i-C8), ammonium hydroxide and Rhodamine B (RhB) dye were provided by SIGMA ALDRICH. Ammonia solution 25% (NH_4OH) was purchased from Merck. Ultrapure water (Millipore Corporation) was used. All reagents were used without further purification.

2.2. Methods

2.2.1. Synthesis of fluorescent silica-coated Au nanoparticles

Fluorescent silica-coated Au nanoparticles were synthesized using microemulsion assisted sol–gel procedure combined with photoreduction reaction (Mihaly et al., 2012). For the synthesis, the ternary system consisting in Brij 30/i-C8/aqueous solution as water-in-oil (W/O) microemulsion was used (Scheme 1). The aqueous solution was obtained by mixing 3-MS (0.1 M) with $HAuCl_4$ (1 g/L) in a 1/3 ratio, and an aqueous solution of RhB dye ($3.15 \cdot 10^{-11}$ mol L^{-1}). The thiol precursor, MS, was used for AuNPs stabilization. After 45 min of mixing, the microemulsion was irradiated with Ultraviolet C (UVC) light (254 nm) for one hour, until the color changes from transparent to yellow showing the formation of Au–MS NPs. Since the Au–silica bond does not occur without a silane coupling agent, various volumes of APTMOS ($7.50 \cdot 10^{-6}$–$7.60 \cdot 10^{-5}$ mol L^{-1}) were used. Then a solution of NH_4OH ($3.50 \cdot 10^{-5}$–$1.41 \cdot 10^{-3}$ mol L^{-1}) and the corresponding TEOS volume in a 2:1 (NH_4OH:TEOS) molar ratio was added and mixed for 30 min in order to obtain different silica shells. The shell thickness was modified from 3 to 116 nm by adjusting the concentration of TEOS in the range $1.61 \cdot 10^{-5}$–$6.40 \cdot 10^{-4}$ mol L^{-1}. The $Au@SiO_2$-RhB NPs were separated by centrifugation (15,000 r.p.m.) from the microemulsion destabilised with acetone and washed five times with acetone (Scheme 1).

RhB dye was physically linked inside the silica shell since the dye was simply dispersed in the initial water-in-oil microemulsion. The encapsulation of RhB dye inside the silica shell has been observed in the washing procedure of core–shell nanoparticles when the supernatant was colourless and the fluorescence signal was absent.

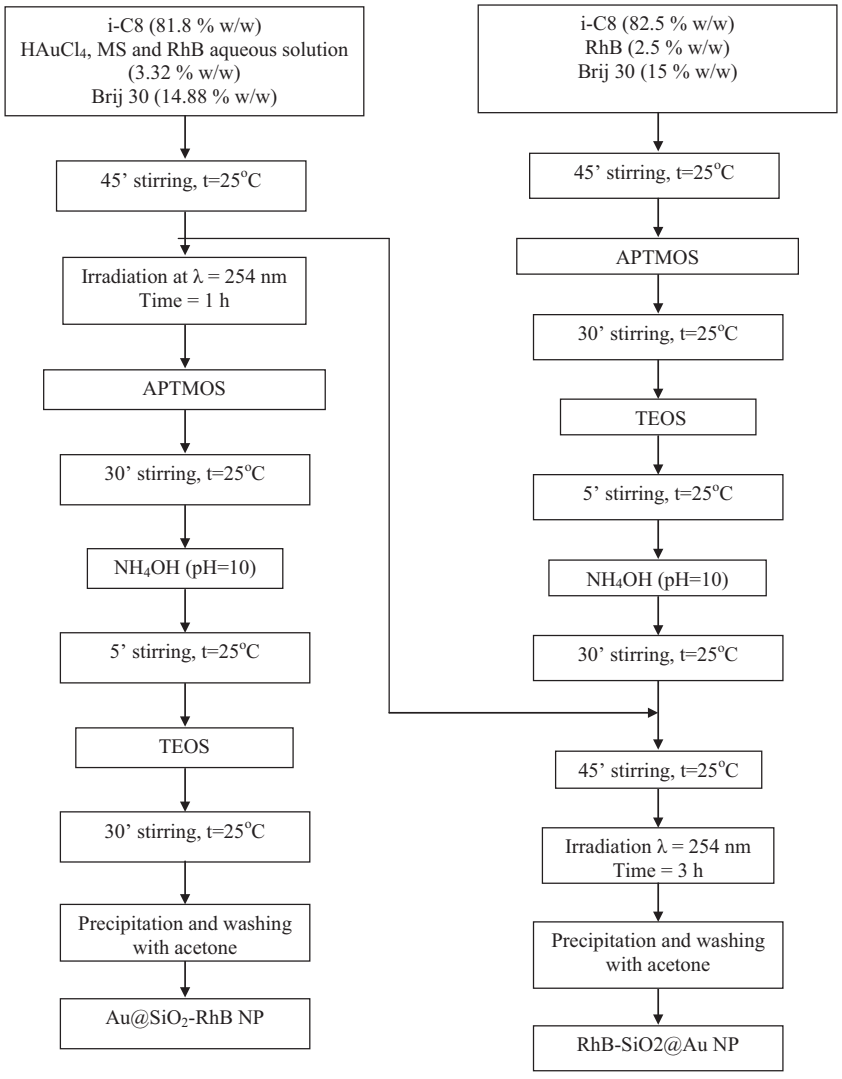

Scheme 1 $Au@SiO_2$-RhB NP and RhB-SiO_2@Au NP synthesis in W/O microemulsion systems.

2.2.2. Synthesis of fluorescent Au-coated silica nanoparticles

Fluorescent Au-coated silica nanoparticles were obtained by mixing two W/O microemulsions (with the same composition used for silica-coated Au nanoparticles), one containing the pre-formed silica network and the other $HAuCl_4$ and MS aqueous solutions. For the synthesis of Au-coated silica nanoparticles a Brij30/i-C8/RhB aqueous solution as W/O microemulsion was used. After 45 min stirring, APTMOS ($2.62 \cdot 10^{-5}$ mol L^{-1}) was added. In this microemulsion, NH_4OH and TEOS ($1.83 \cdot 10^{-4}$ mol L^{-1}) in a 2:1 M ratio were subsequently added. In order to obtain Au-coated silica nanoparticles with different gold shell sizes various concentrations of $HAuCl_4$ ($8.3 \cdot 10^{-4}$–$1.4 \cdot 10^{-3}$ mol L^{-1}) were used. After mixing the two microemulsions for 45 min, the final system was irradiated in a photoreactor with a UVC light for three hours. The recuperation of the RhB-SiO_2@Au NP was realized in the same way as for $Au@SiO_2$-RhB NP.

2.2.3. Irradiation equipment

A Luzchem photoreactor, LZC-4X, equipped with eight lamps, each of 12 W (using UVC – 254 nm), was used for the synthesis of gold nanoparticles. The intensity per each lamp was 0.024 W/m^2. Constant stirring of the solution was ensured by using a magnetic stirrer. The temperature was kept constant throughout the reaction time by the ventilation system in the main chamber.

2.2.4. Characterization techniques

The size measurements of nanoparticles in pristine microemulsion were performed on a Malvern Nanosizer Equipment (NANO-ZS) based on Dynamic Light Scattering (DLS) principle, at 90° scattered light. All the measurements were done in triplicate at 25 °C constant temperature. The spectral characterization of $Au@SiO_2$-RhB NP and RhB-SiO_2@Au NP as powders was evaluated using a Jasco V-670 spectrophotometer. The X-ray diffraction pattern of fluorescent nanoparticles as powders was obtained using a Shimadzu XRD 6000 diffractometer. Transmission Electron Microscopy (TEM) and High-Resolution Transmission Electron Microscopy (HR-TEM) micrographs coupled with selected area diffraction (SAED) and Energy-Dispersive X-ray (EDX) microanalysis were performed on a Tecnai G2F30 S – TWIN model. The scanning

electron images were obtained by using a Quanta Inspect F microscope, with a field emission gun (FEG) which has a resolution of 1.2 nm and equipped with an EDAX spectrometer with a resolution at MnK of 133 eV. A Jasco FP-6500 spectrofluorometer was used for fluorescence spectra registration of Au@SiO_2-RhB and RhB-SiO_2@Au NPs. The excitation wavelength in experiments was fixed at 450 nm in accordance with the RhB absorbance peak.

3. Results and discussion

3.1. The characterization of the fluorescent core–shell nanoparticles

3.1.1. DLS measurements

Fig. 1a shows that the microemulsion template applied for Au@SiO_2-RhB NPs, before the addition of TEOS and NH_4OH, contains structural units similar in size and shape. The initial size of AuNP stabilized with MS thiol in microemulsion was around 8 nm. Au@SiO_2-RhB NPs with sizes in the range 14–240 nm corresponding to silica shells thickness between 3–116 nm were obtained (Table 1). RhB-SiO_2@Au NPs with sizes from 26 to 96 nm were also synthesized (Fig. 1b, Table 1).

Both core–shell structures, Au@SiO_2-RhB and RhB-SiO_2@Au NPs synthesized in the W/O microemulsion showed a narrow pore size distribution (with polydispersity values smaller than 0.250) thus confirming the high degree of homogeneity of these nano-dispersed systems.

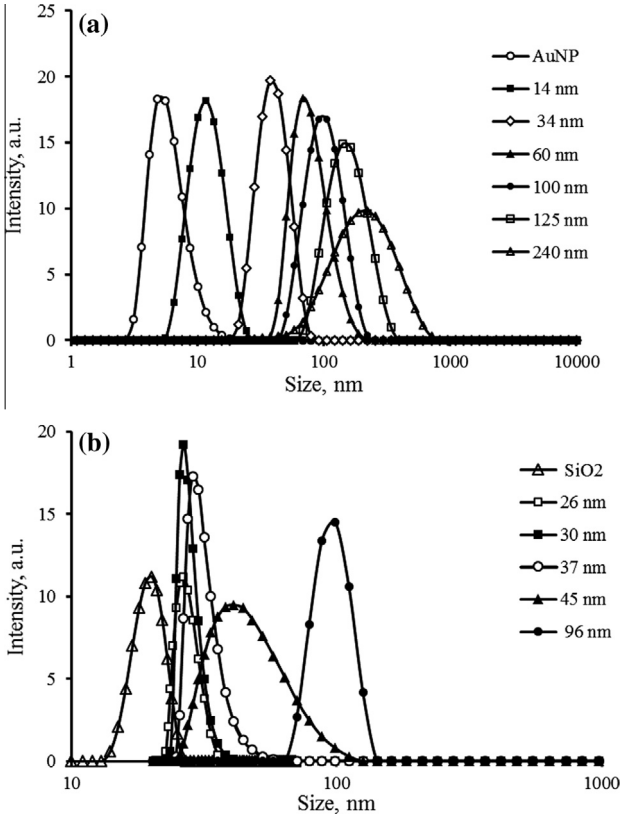

Figure 1 Size measurements for: (a) Au@SiO_2-RhB NP and (b) RhB-SiO_2@Au NP core–shell nanostructures.

This size evolution of the two types of core–shell nanostructures can be interpreted in tight connection with their electronic spectra.

3.1.2. UV–VIS absorbance spectra

For core–shell nanoparticles synthesis, the thiol (3-MS) was added to functionalize the surfaces of AuNPs by thiol molecules. By adding APTMOS, some 3-MS molecules adsorbed on the surface of AuNP were replaced by APTMOS molecules as the N–Au bonds are stronger than S–Au. Then the UV–VIS spectra of core–shell nanostructures were registered. In Fig. 2a are shown the UV–VIS spectra of pure AuNPs with and without the outer protecting SiO_2 shell. No obvious peak was evidenced within the investigated wavelength range (λ = 400–700 nm) for SiO_2 nanoparticles. For Au@SiO_2 nanoparticles a peak around 530 nm can be seen distinctly originating from the AuNPs inside the core–shell structures. With the increase of TEOS volume (Table 1), the plasmon resonance bands appear at the same wavelength, behaviour which is similar with that of Au nanoparticles observed in ethanol (Daniel and Astruc, 2004). As the silica shells are optically transparent, UV–VIS measurements detect mainly the electronic bands of the inner AuNPs. Therefore, the plasmon resonance bands of the samples synthesized with constant $HAuCl_4$ and different TEOS and NH_4OH volumes appears at the same wavelength (525 nm) (Erni and Browning, 2007). The narrow absorption band of Au@SiO_2 NPs also indicates that the nanoparticles are well dispersed as a result of electrostatic repulsion arising from the electrical double layer around the Au NPs (Chegel et al., 2012).

Au nanoparticles with an average diameter of about 8 nm have a surface plasmon resonance (SPR) at wavelength of approximately 525 nm (Link and El Sayed, 2000) (Fig. 2b). With SiO_2 nanoparticles inside, the SiO_2@Au core–shell structures exhibit a well-defined absorption peak between 546 and 605 nm with increasing the gold shell by modifying $HAuCl_4$ from 0.83 mmol L^{-1} to 1.4 mmol L^{-1}. When the concentration of $HAuCl_4$ is 0.83 mmol L^{-1}, it produces a plasmon resonance peak at 546 nm. By increasing the $HAuCl_4$ concentration (1 mmol L^{-1}), the plasmon resonance band broadens and displays a red shift (566 nm), indicating the formation of SiO_2@Au with higher gold shell. When the concentration of $HAuCl_4$ is increasing to 1.4 mmol L^{-1}, the VIS absorption curve becomes very broad and the maximum absorbance peak shifts to 605 nm with a very low intensity due to the formation of larger gold shells.

3.1.3. XRD analysis

The final Au@SiO_2-RhB NPs, as powder, were further subjected to XRD measurements. In Fig. 3 the XRD data for Au@SiO_2-RhB NPs with sizes of 60 nm are represented. In general, SiO_2 shows a broad amorphous feature at 2θ (44°–77.74°). Au peaks appear at 2θ 38°, 44°, 65°, and 78°, corresponding to gold (111), (200), (220) and (311), respectively (Quyen et al., 2014). These peaks are consistent with the Joint Committee on Powder Diffraction Standard (JCPDS 04-0784). On the other hand, SiO_2 maintains its amorphous phase and the formation of new phases is not detected. For RhB-SiO_2@Au NPs a similar crystalline structure was obtained and therefore, the corresponding XRD pattern was not presented.

Table 1 Experimental condition for obtaining Au@SiO_2-RhB NP and RhB-SiO_2@Au NP core–shell nanoparticles with different silica and Au shells.

Au@SiO_2-RhB NP					RhB-SiO_2@Au NP		
Sample	Silica shell (nm)	APTMOS concentration (10^5 mol L^{-1})	TEOS concentration (10^5 mol L^{-1})	NH_4OH concentration (10^5 mol L^{-1})	Sample	Au shell, nm	$HAuCl_4$ concentration (10^3 mol L^{-1})
S1	3	0.75	1.61	3.50	S7	3	0.83
S2	13	1.52	4.00	8.80	S8	5	1.00
S3	26	3.05	8.00	17.60	S9	8.5	1.18
S4	46	4.57	16.00	35.20	S10	12.5	1.30
S5	58.5	6.10	32.00	70.40	S11	38	1.40
S6	116	7.60	64.00	140.80			

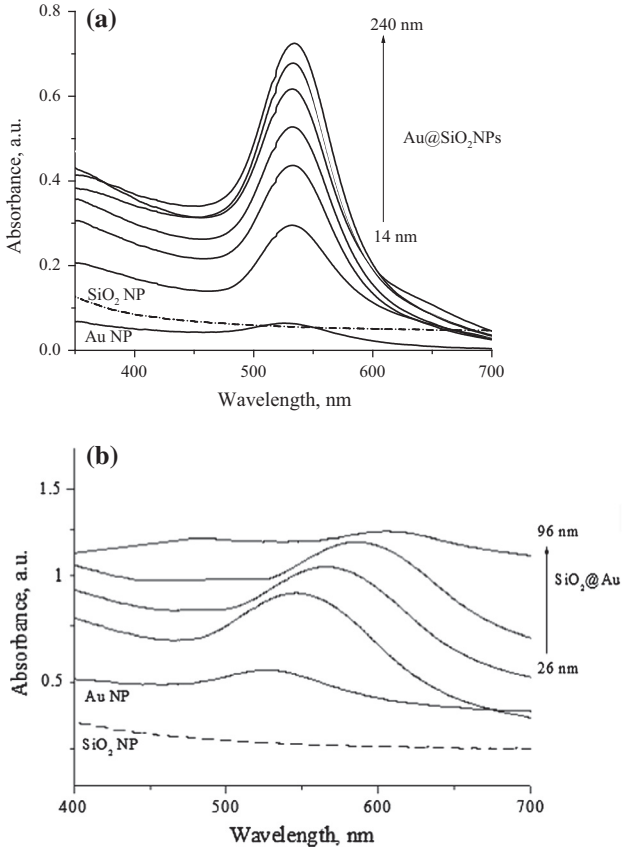

Figure 2 UV–VIS absorbance spectra of Au@SiO_2 (a) and SiO_2@Au (b) core–shell nanostructures.

3.1.4. Topographic structure

The morphology and size of as-prepared Au@SiO_2-RhB and RhB-SiO_2@Au core–shell NPs were measured by TEM, HR-TEM and SEM analyses (Fig. 4a–h). In the case of Au@SiO_2-RhB NPs the average diameter of AuNP (stabilized with 3-MS thiol) core and the thickness of SiO_2 shell are approximately 3 nm and 12 nm, respectively (Fig. 4b). TEM images showed smaller sizes for the nanoparticles than DLS measurements due to the hydration water that was eliminated during the air drying process. The Au@SiO_2-RhB NPs were spherical with smooth surface.

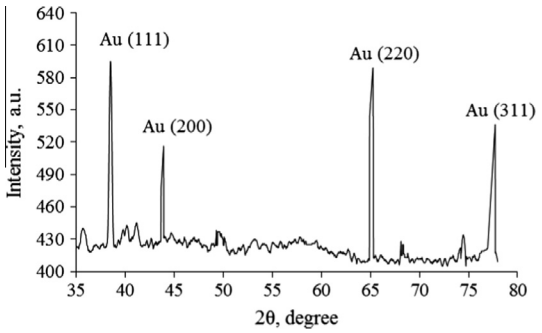

Figure 3 XRD pattern of RhB-SiO_2@Au NPs.

In the HR-TEM images of SiO_2@Au NP and RhB-SiO_2@Au NP, the SiO_2 NPs encapsulating RhB dye have sizes around 20 nm, whereas small Au NP, around 5 nm are attached to the SiO_2 NP surface. The morphology of RhB-SiO_2@Au NP revealed by HR-TEM microscopy was confirmed by the SEM analysis (Fig. 4h).

SAED analysis indicated the existence of the crystallinity planes corresponding to Au (1 1 1) for both Au@SiO_2-RhB and RhB-SiO_2@Au NPs.

SEM images of the prepared samples (Au@SiO_2-RhB and RhB-SiO_2@Au NPs) have been performed in order to determine the surface morphology and are shown in Fig. 4g and h. The core–shell structure of prepared samples can easily be noticed as well as their spherical and uniform shapes. For RhB-SiO_2@Au NP may also be observed the brightest spots due to the AuNP attached to the SiO_2 surface.

More SiO_2 or Au NPs shells are presented in supporting information (Fig. 1). It can be noticed that for SiO_2@Au NP the silica NPs are decorated with more or less Au NPs (Figs. 4d and e and 1c and d from supporting information), results that are in good agreement with other studies regarding the SiO2@Au NPs core–shell nanostructures (Choma et al., 2011; Luo et al., 2013; Saini et al., 2015).

In the EDX spectra of the core–shell nanoparticles (Fig. 5), all characteristic peaks were well matched with their unique elements of Au, O, C and Si. The Cu peaks occurred due to the supporting substrate used for TEM sampling. Furthermore, quantitative elemental analyses of the core–shell nanoparticles are listed in Table 2. This was in good agreement with the elemental peaks presented in Fig. 5.

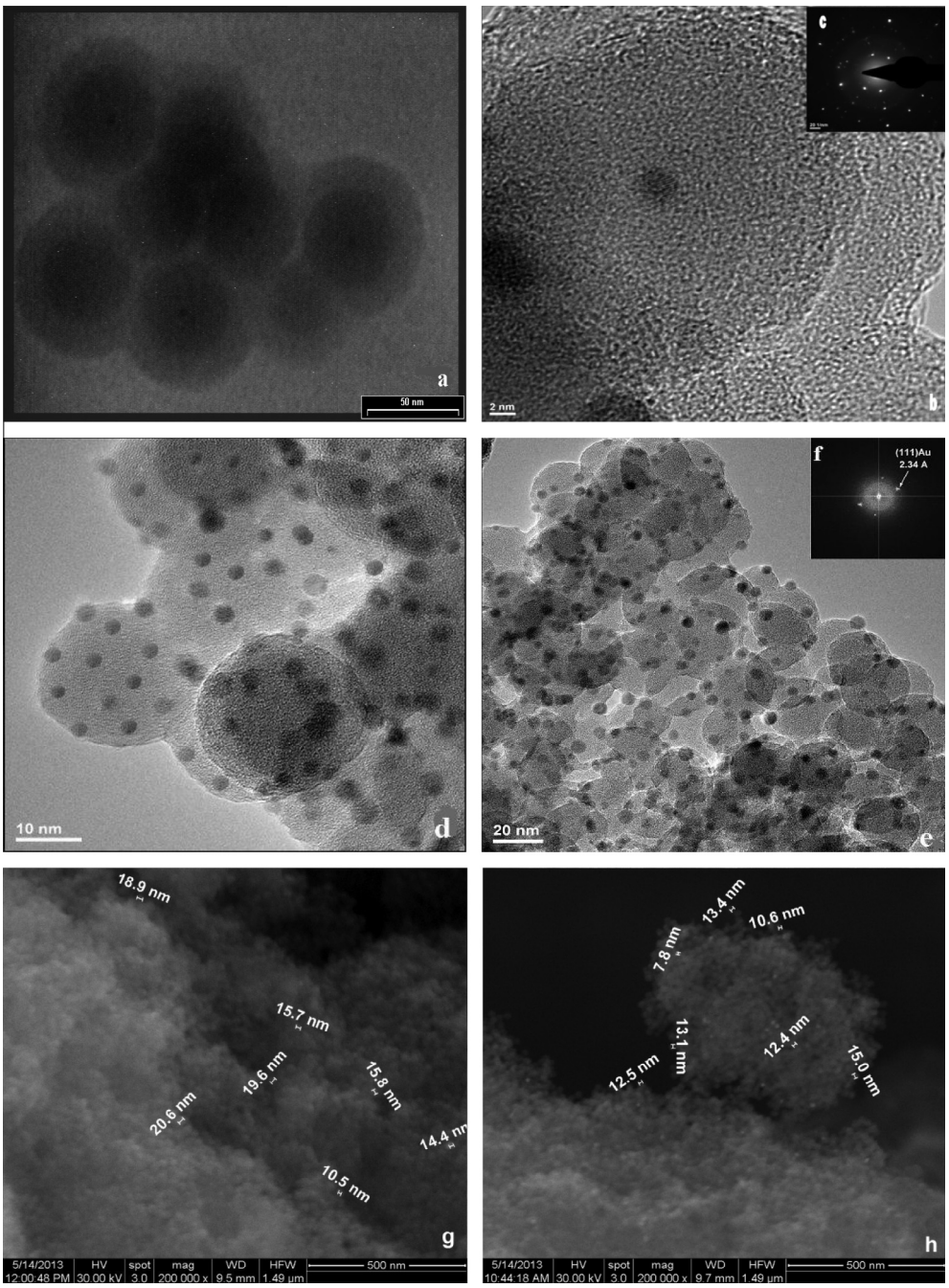

Figure 4 TEM (a), HR-TEM (b, d, and e), SAED (c and f) and SEM (g and h) micrographs of: (a) RhB-Au@SiO_2 NP (S3); (b) Au@SiO_2NP (S2); (c) the inset shows the corresponding SAED pattern of Au@SiO_2 NP (S2); (d) SiO_2@Au NP (S7); (e) RhB-SiO_2@Au NP (S8); (f) the inset shows the corresponding SAED pattern of RhB-SiO_2@Au NP (S8); (g) RhB-Au@SiO_2 NP (S3)and (h) RhB-SiO_2@Au NP (S8).

3.2. Fluorescence enhancement of Au@SiO_2-RhB NP and RhB-SiO_2@Au NP

3.2.1. Characterization of Au@SiO_2-RhB NP with different silica shells

In order to observe the fluorescence enhancement of Au@SiO_2NP over RhB dye, several silica-coated Au nanoparticles with different silica shell sizes were synthesized by modification of silica precursor (TEOS) concentration into the initial reaction media. Then Au@SiO_2-RhB NPs were characterized by fluorescence analysis.

In Fig. 6 are presented the fluorescence spectra of Au@SiO_2-RhB NPs with different silica shells measured in microemulsion and in solid phase. As the concentration of TEOS in reaction media increases from $1.61 \cdot 10^{-5}$ to $6.40 \cdot 10^{-4}$ mol L^{-1}, the peak fluorescence intensity and nanoparticles size are raising consequently (Fig. 6a). The fluorescence intensity of Au@SiO_2-RhB NPs was raised up to 5

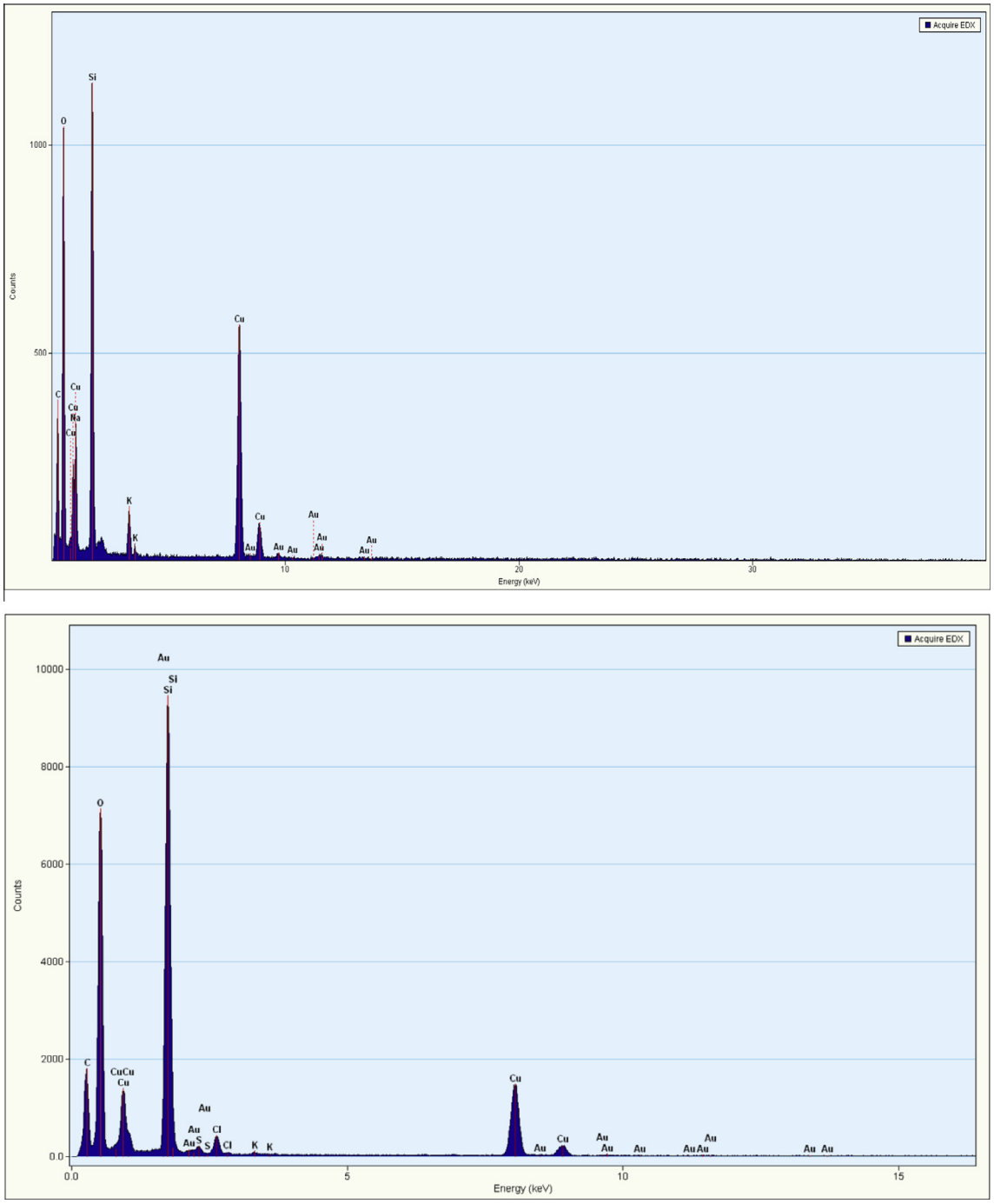

Figure 5 EDX spectra of Au@SiO_2-RhB NP (upper side-corresponding to Fig. 4b) and RhB-SiO_2@Au NP (bottom side-corresponding to Fig. 4e).

times compared to simple AuNPs. Thus, by raising the silica shell size the fluorescence signal increases. Likewise, since the fluorescence intensity increased proportionally with TEOS amount in reaction media one may affirm that the RhB dye is oriented inside the silica shell thus acting like a spacer between AuNP and RhB dye. These results have been also confirmed by the fluorescence measurements in solid phase (Au@SiO_2-RhB powder) obtained after breaking the microemulsion with acetone (Fig. 6b). Similar results were obtained by Huang et al. (2013). They observed that the fluorescence quenching evolution of FITC (fluorescein isothiocyanate) dye inside Au@SiO_2@FITC nanoparticles is no longer carried out as the silica shell is growing.

When comparing the fluorescence enhancement of two types of NPs the confinement of RhB inside SiO_2 matrix is more efficient whether it is in the core than in the particle shell, fluorescence values being one magnitude order higher for RhB-SiO_2@Au than for Au@SiO_2-RhB NPs.

Table 2 The percentage elemental composition of core–shell nanoparticles from EDX analyses.

NP	Element	Atom%
Au@SiO_2-RhB	Cu K	18.00
	C K	12.17
	O K	31.08
	Si K	38.28
	Au K	0.47
RhB-SiO_2@Au	Cu K	7.69
	C K	9.34
	O K	35.71
	Si K	46.71
	Au K	0.56

3.2.2. Characterization of RhB-SiO_2@AuNP with different AuNP shells

Fluorescence spectra of RhB-SiO_2@Au NP with different AuNP shells in microemulsion and solid phase are presented in Fig. 7a and b. It can be noticed that, as the AuNP shell increases covering the silica core the fluorescence signal increases as well.

As the gold concentration increases, the relative amount of the AuNPs entering the plasmonic enhancement region of RhB-SiO_2@Au NP is growing, and thus the fluorescence signal grows accordingly. As the gold concentration increases further, the fluorescence signal begins to show a relatively slow growing process. This fluorescence quenching can be ascribed to the dominant fluorescence effect caused by superfluous SiO_2@Au NPs with respect to the number of free AuNPs. One can also see from the fluorescence spectra of RhB-SiO_2@Au NP that the peak was red-shifted from 575 to 585 nm as the gold coating increases. Initially, less number of gold nanoparticles was attached to silica core and the number of coatings increases the gold particles which smoothly cover almost the whole surface of silica, which shows large measurable red shift in peak. As the shell thickness increased, the fluorescence peak started to shift toward lower wavelength (582 nm).

3.2.3. Quantitative parameters of fluorescence enhancement

The fluorescence enhancement by Au nanoparticles was described by fluorescence enhancement factor, F ($F = I_1/I_0$), where I_1 is the fluorescence intensity of Au@SiO_2-RhB core–shell NPs per unit SiO_2 volume (I_1 is increased intensity/increased volume and I_0 is the fluorescence intensity of

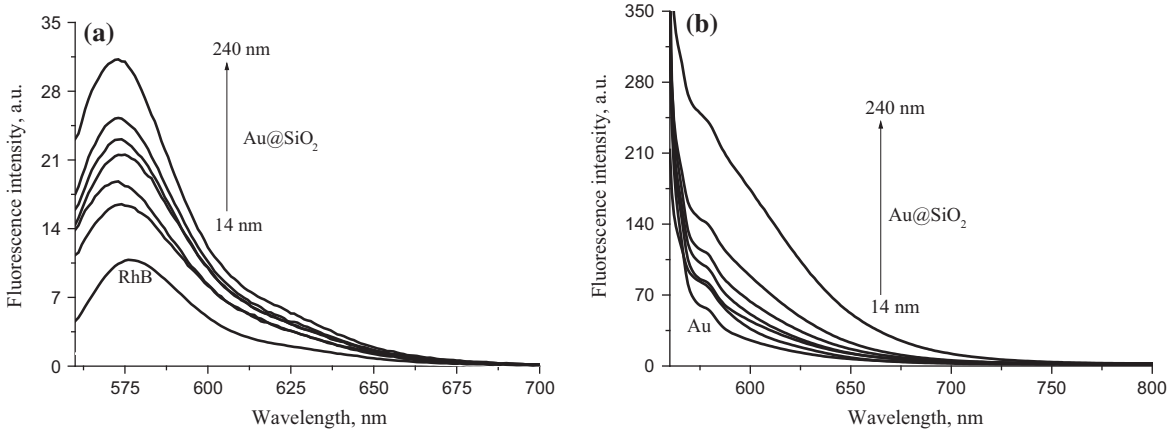

Figure 6 Fluorescence spectra of Au@SiO_2-RhB NPs with different silica shell sizes measured in: (a) microemulsion and (b) solid phase.

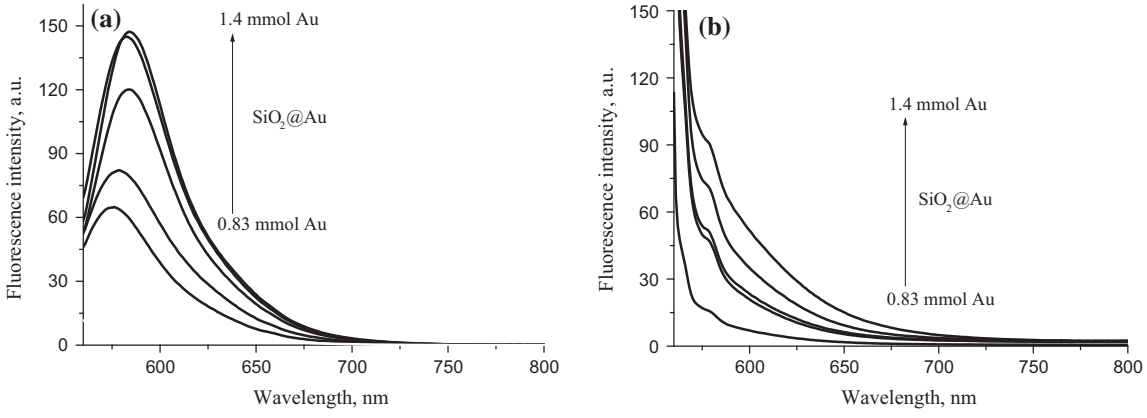

Figure 7 Fluorescence spectra of RhB-SiO_2@Au NPs with different AuNPs shell measured in: (a) microemulsion phase and (b) solid phase.

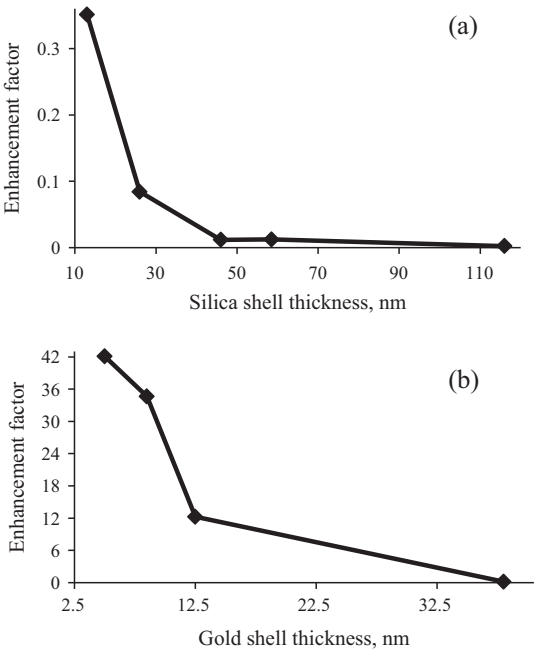

Figure 8 The enhancement factor for Au@SiO_2-RhB and RhB-SiO_2@Au nanoparticles compared with RhB-SiO_2 and RhB-Au without Au core or SiO_2 core.

RhB-SiO_2 spheres without Au core per unit SiO_2 volume ($I_0 = 8.57 \cdot 10^{-15}$ nm^{-3})). This calculus was also done for RhB-SiO_2@Au NPs. The enhancement factors for Au@SiO_2-RhB and RhB-SiO_2@Au NPs were plotted against silica shell thickness, based on the calculation reported in Supporting Information (Tables 1 and 2). The values of F decreased sharply with increasing silica shell thickness, as shown in Fig. 8a. This is also valid for RhB-SiO_2@Au NPs with increasing gold shell. Thus these results indicate that the extent of influence by Au nanoparticles on the fluorescence of RhB is significant for a shell thickness less than 50 nm in the case of Au@SiO_2-RhB and 15 nm for SiO_2@Au NPs. This was also observed by Li and Zhu (2013) who instead of RhB and 8 nm of Au NP, they used OG-488 fluorophores and bigger Au nanoparticles (40, 60, 80 nm) and Chen et al. (2013) who developed nanocomposites with bigger Au cores (13.7 nm) covered by a thin PVP coating layer a silica spacer and a fluorescent dye (TAMRA) layer in the silica matrix. The explanation of such behaviour can be described as follows: in the case of Au@SiO2-RhB NPs the absorption of light by AuNPs which favours the enhancement fluorescence is hindered by RhB dye which in the case of SiO_2@Au NPs is not valid. Also, the decoration of AuNPs onto the silica surface enables light to reach the Au and RhB dye with enhanced fluorescence and the compact silica-RhB shell covering the AuNPs surface obtained by polymerization prevents the light to reach AuNPs.

The increasing thickness of the SiO_2 shell layer reduces the material surface activity of the core surface; as a result, quantum yield of Au@SiO_2 also reduces (Fig. 9). This is due to the quenching effect of metal nanoparticles on nearby fluorescent dye through a non-radiative energy transfer manner, because of surface plasmon resonance of gold (Dubertret et al., 2001). The manner of quantum yield calculation is presented in Supporting Information.

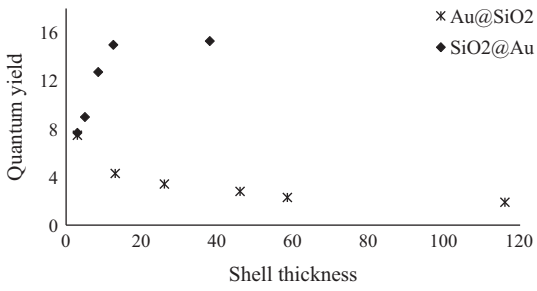

Figure 9 Quantum yield dependence on the shell thickness for Au@SiO_2 and SiO_2@Au.

As for SiO_2@Au as the light-emitter is placed close to the plasmons, the light-emitter excitation rate will be enhanced when the wavelength of the plasmon resonance is close to the excitation wavelength of the light-emitter and as such the quantum yield will increase (Fig. 9). When Au gets close to the RhB molecule, the fluorescence intensity continuously increases and reaches a maximum at a distance of $z = 5$ nm. During this process, the excitation rate is enhanced. At the same time, the overall quantum yield also increases because of the faster increasing speed of the radiative decay rate as compared to that of the non-radiative decay. However, the non-radiative decay rate will increase rapidly if the distance z becomes even smaller, moment at which fluorescence quenching occurs (Ji, 2014).

4. Conclusions

A detailed analysis on correlation between size measurements and spectral characteristics allows highlighting the following aspects:

- versatility of microemulsion assisted sol–gel method coupled with photoreduction reaction able to produce complex noble metal/SiO_2 NPs when the roles of core and shell are interchangeable;
- possibility to conduct the synthesis in a "one-pot" procedure, making thus the route very advantageous over other synthesis procedures, being less time consuming, and reducing the amount of chemicals;
- ability to enhance the dye fluorescence by tuning silica and gold shell thickness and thus to obtain materials with tailored properties adequate to purpose.

HR-TEM micrographs confirmed the structure of both core–shell nanostructures and the results were in good agreement with DLS measurements. It was noticed that the fluorescence enhancement of RhB dye depends on Au and silica shell thickness, the fluorescence signal being one magnitude order higher in the former case.

Further studies will be performed to complete these linear optical properties (UV–VIS, fluorescence) with non-linear properties (NLO), such as third harmonics generation (THG) (Bazaru Rujoiu et al., 2015).

Acknowledgement

This work was done in the frame of the Program: Cooperation in Priority Fields – PNII, developed with the support of ANCS, CNDI-UEFISCDI, Romania, in the project SimFotoAd, PN-II-PT-PCCA-2013-4-0726, contract no. *217/2014*.

Appendix A. Supplementary material

Supplementary data associated with this article can be found, in the online version, at http://dx.doi.org/10.1016/j.arabjc.2015.12.014.

References

Amjadi, M., Farzampour, L., 2014. Fluorescence quenching of fluoroquinolones by gold nanoparticles with different sizes and its analytical application. J. Lumin. 145, 263–268.

Bazaru Rujoiu, T., Petris, A., Vlad, V.I., Rau, I., Manea, A.M., Kajzar, F., 2015. Lasing in DNA-CTMA doped with Rhodamine 610 in butanol. Phys. Chem. Chem. Phys. 17 (19), 13104–13111.

Chandrasekharan, N., Kamat, P.V., Hu, J., Jones, G., 2000. Dye-capped gold nanoclusters: photoinduced morphological changes in gold/Rhodamine 6G nanoassemblies. J. Phys. Chem. B 104, 11103–11109.

Chegel, V., Rachkov, O., Lopatynski, A., Ishihara, S., Yanchuk, I., Nemoto, Y., Hill, J.P., Ariga, K., 2012. Gold nanoparticles aggregation: drastic effect of cooperative functionalities in a single molecular conjugate. J. Phys. Chem. C 116, 2683–2690.

Chen, J., Jiang, J., Gao, X., Gong, J., Shen, G., Yu, R., 2007a. Gold-aggregated, dye-embedded, polymer-protected nanoparticles (GDPNs): a new type of tags for detection with SERS. Coll. Surf. A: Physicochem. Eng. Aspects 294, 80–85.

Chen, J., Zheng, A., Chen, A., Gao, Y., He, C., Kai, X., Wu, G., Chen, Y., 2007b. A functionalized gold nanoparticles and Rhodamine 6G based fluorescent sensor for high sensitive and selective detection of mercury(II) in environmental water samples. Anal. Chem. Acta 599, 134–142.

Chen, J., Jin, Y., Fahruddin, N., Zhao, J.X., 2013. Development of gold nanoparticle-enhanced fluorescent nanocomposites. Langmuir 29, 1584–1591.

Choma, J., Dziura, A., Jamiola, D., Nyga, P., Jaroniec, M., 2011. Preparation of silica–gold core–shell particles. Colloid Surf. A: Physicochem. Eng. Aspects 373, 167–171.

Daniel, M.C., Astruc, D., 2004. Gold nanoparticles: assembly, supramolecular chemistry, quantum-size-related properties, and applications toward biology, catalysis, and nanotechnology. Chem. Rev. 104, 293–346.

Dong, L., Ye, F., Hu, J., Popov, S., Muhammed, M., 2011. Fluorescence quenching and photobleaching in Au/Rh 6G nanoassemblies: impact of competition between radiative and non-radiative decay. J. Eur. Opt. Soc. Rapid Publ. 6, 11019-1-6.

Dong, L., Yi, F., Chughtai, A., Popov, S., Friberg, A.T., Muhammed, M., 2012. Photostability of lasing process from water solution of Rhodamine 6G with gold nanoparticles. Opt. Lett. 37, 34–36.

Dubertret, B., Calame, M., Libchaber, A.J., 2001. Single-mismatch detection using gold-quenched fluorescent oligonucleotides. Nat. Biotechnol. 19, 365–370.

Erni, R., Browning, N.D., 2007. Quantification of the size-dependent energy gap of individual Cd, Se quantum dots by valence electron energy-loss spectroscopy. Ultramicroscopy 107, 267–273.

Geddes, C.D., Lakowicz, J.R., 2002. Metal-enhanced fluorescence. J. Fluorescence 12, 121–129.

Hayashi, K., Nakamura, M., Ishimura, K., 2013. Near-infrared fluorescent silica-coated gold nanoparticle clusters for X-ray computed tomography/optical dual modal imaging of the lymphatic system. Adv. Healthc. Mater. 2, 756–763.

Huang, Y.F., Ma, K.H., Kang, K.B., Zhao, M., Zhang, Z.L., Liu, Y. X., Wen, T., Wang, Q., Qiu, W.Y., Qiu, D., 2013. Core–shell plasmonic nanostructures to fine-tune long "Au nanoparticle-fluorophore" distance and radiative dynamics. Colloids Surf. A: Physicochem. Eng. Aspects 421, 101–108.

Ji Botao, 2014. Synthesis and Optical Properties of Plasmonic Fluorescent Quantum Dots. Material chemistry. Universitе Pierre et Marie Curie – Paris VI, English.

Kinkhabwala, A., Yu, Z.F., Fan, S.H., Avlasevich, Y., Mullen, K., Moerner, W.E., 2009. Large single-molecule fluorescence enhancements produced by a bowtie nanoantenna. Nat. Photon. 3, 654–657.

Knopp, D., Tang, D., Niessner, R., 2009. Review: bioanalytical applications of biomolecule-functionalized nanometer-sized doped silica particles. Anal. Chim. Acta 647 (1), 14–30.

Larson, D.R., Zipfel, W.R., Williams, R.W., Clark, S.W., Bruchez, M. P., Wise, F.W., Webb, W.W., 2003. Water-soluble quantum dots for multiphoton fluorescence imaging in vivo. Science 300, 1434–1436.

Li, C., Zhu, J., 2013. Metal-enhanced fluorescence of OG-488 doped in Au@SiO_2 core–shell nanoparticles. Mater. Lett. 112, 169–172.

Link, S., El Sayed, M.A., 2000. Shape and size dependence of radiative, non-radiative and photothermal properties of gold nanocrystals. Int. Rev. Phys. Chem. 19, 409–453.

Lu, H., Ju, H.F., Yang, Q., Li, Z.R., Ren, H.Y., Xin, X., Xu, G.Y., 2013. Synthesis of Ag@SiO2 hybrid nanoparticles templated by a Triton X-100/1-hexanol/cyclohexane/H_2O water-in-oil microemulsion. Cryst. Eng. Commun. 15, 6511–6517.

Luo, D., Han, E., Belcheva, N., Saltzman, W.M., 2004. A self-assembled, modular DNA delivery system mediated by silica nanoparticles. J. Control Release 95 (2), 333–341.

Luo, J., Chu, W., Sall, S., Petit, C., 2013. Facile synthesis of monodispersed Au nanoparticles coated on Stober silica. Colloid Surf. A: Physicochem. Eng. Aspects 425, 83–91.

Miao, Y., Gan, N., Li, T., Cao, Y., Hu, F., Chen, Y., 2016. An ultrasensitive fluorescence aptasensor for chloramphenicol based on FRET between quantum dots as donor and the magnetic SiO_2@Au NPs probe as acceptor with exonuclease-assisted target recycling. Sensors Actuators B 222, 1066–1072.

Mihaly, M., Fleancu, M.C., Olteanu, N.L., Bojin, D., Meghea, A., Enachescu, M., 2012. Synthesis of gold nanoparticles by microemulsion assisted photoreduction method. C. R. Chimie 15, 1012–1021.

Narband, N., Uppal, M., Dunnill, C.W., Hyett, G., Wilson, M., Parkin, I.P., 2009. The interaction between gold nanoparticles and cationic and anionic dyes: enhanced UV–visible absorption. Phys. Chem. Chem. Phys. 11, 10513–10518.

Pak, J., Yoo, H., 2013. Facile synthesis of spherical nanoparticles with a silica shell and multiple Au nanodots as the core. J. Mater. Chem. A 1, 5408–5413.

Popov, O., Zilbershtein, A., Davidov, D., 2006. Enhanced gain at the surface-plasmon-resonance wavelength. Appl. Phys. Lett. 89, 191116-1-3.

Quyen, T.T.B., Chang, C.C., Su, W.N., Uen, Y.H., Pan, C.J., Liu, J. Y., Rick, J., Lin, K.Y., Hwang, B.J., 2014. Self-focusing Au@SiO_2 nanorods with Rhodamine 6G as highly sensitive SERS substrate for carcinoembryonic antigen detection. J. Mater. Chem. B 2, 629–636.

Ren, Y.J., Xin, X., Tang, W.Y., Zhang, Y.J., Shen, J.L., Wang, L., 2015. Reverse microemulsion-mediated synthesis of Au@SiO_2 hybrid nanoparticles with different morphologies. Colloid Polym. Sci. 293, 1695–1703.

Rigo, M.V., Seo, J., Kim, W., Jung, S., 2011. Plasmon coupling of R6G-linked gold nanoparticle assemblies for surface-enhanced Raman spectroscopy. Vib. Spectrosc. 57, 315–318.

Rossi, L.M., Shi, L., Quina, F.H., Rosenzweig, Z., 2005. Stöber synthesis of monodispersed luminescent silica nanoparticles for bioanalytical assays. Langmuir 21 (10), 4277–4280.

Saini, A., Maurer, T., Izquierdo Lorenzo, I., Ribeiro Santos, A., Beal, J., Goffard, J., Gerard, D., Vial, A., Plain, J., 2015. Synthesis and SERS application of SiO_2@Au nanoparticles. Plasmonics 10, 791–796.

Sathiyamoorthy, K., Sreekanth, K.V., Sidharthan, R., Murukeshan, V.M., Xing, B., 2011. Surface plasmon enhancement in gold nanoparticles in the presence of an optical gain medium: an analysis. J. Phys. D: Appl. Phys. 44, 425102.

Sen, T., Patra, A., 2008. Resonance energy transfer from Rhodamine 6G to gold nanoparticles by steady-state and time-resolved spectroscopy. J. Phys. Chem. C 112, 3216–3222.

Sen, T., Patra, A., 2009. Formation of self-assembled au nanoparticles and the study of their optical properties by steady-state and time-resolved spectroscopies. J. Phys. Chem. C 113, 13125–13132.

Törngren, B., Akitsu, K., Ylinen, A., Sandén, S., Jiang, H., Ruokolainen, J., Komatsu, M., Hamamura, T., Nakazaki, J., Kubo, T., Segawa, H., Österbacka, R., Smått, J.-H., 2014. Investigation of plasmonic gold–silica core–shell nanoparticle stability in dye-sensitized solar cell applications. J. Colloid Interface Sci. 427, 54–61.

Wang, Y., Zhou, X., Wang, T., Zhou, J., 2008a. Enhanced luminescence from lanthanide complex by silver nanoparticles. Mater. Lett. 62, 3582–3584.

Wang, Y., Zhou, J., Wang, T., 2008b. Enhanced luminescence from europium complex owing to surface plasmon resonance of silver nanoparticles. Mater. Lett. 62, 1937–1940.

Wang, Q., Lin, S., Ming, C., Zhao, H., Liu, J., Zhang, C., Song, F., Pun, E.Y.B., 2011. Plasmon-enhanced luminescence of Eu complex by using silver nanocubes for different excitations. Mater. Lett. 65, 905–907.

Yan, J., Estévez, M.C., Smith, J.E., Wang, K., He, X., Wang, L., et al, 2007. Dye-doped nanoparticles for bioanalysis. Nano Today 2 (3), 44–50.

Zhu, S.G., Xiang, J.J., Li, X.L., Shen, S.R., Lu, H., Zhou, J., et al, 2004. Poly(l-lysine)-modified silica nanoparticles for the delivery of antisense oligonucleotides. Biotechnol. Appl. Biochem. 39 (2), 179–187.